Uniformity of Large-Area Bilayer Graphene Grown by Chemical Vapour Deposition

Yuewen Sheng,[1] Youmin Rong,[1] Zhengyu He,[1] Ye Fan,[1] Jamie H. Warner[1]*

[1]Department of Materials, University of Oxford, Parks Road, Oxford, OX1 3PH, UK

*Jamie.Warner@materials.ox.ac.uk

Keywords Graphene, bilayer, chemical vapor deposition, large area, uniformity, transparent conducting electrode.

Abstract

Graphene grown by chemical vapour deposition (CVD) on copper foils is a viable method for large area films for transparent conducting electrode (TCE) applications. We examine the spatial uniformity of large area films on the centimeter scale when transferred onto both Si substrates with 300nm oxide and flexible transparent PET substrates. A difference in the quality of graphene, as measured by the sheet resistance and transparency, is found for the areas at the edges of large sheets that depends on the supporting boat used for the CVD growth. Bilayer graphene is grown with uniform properties on the centimeter scale when a flat support is used for CVD growth. The flat support provides consistent delivery of precursor to the copper catalyst for graphene growth. These results provide important insights into the upscaling of CVD methods for growing high quality graphene and its transfer onto flexible substrates for potential applications as a TCE.

Graphene is a two-dimensional carbon material that is only one atom thick, first isolated in 2004 by mechanical exfoliation.[1] Its extended honeycomb network is the basic building block of other important carbon materials: 3D graphite, 1D nanotubes and 0D fullerenes.[2,3] Graphene has attracted interest due to its special properties, including high charge carrier mobility and charge carrier density, high optical transmittance and excellent thermal conductivity.[4–6] It is believed to have potential for various applications, which include high-speed and radio frequency logic devices, sensors, and TCE for displays, touch screens, LEDs and solar cells.[7–13]

The micromechanical cleavage of graphite to isolate graphene is not compatible with large area TCE applications. Alternative methods[14–19] have been developed to achieve reliable and repeatable synthesis of large-area graphene sheets up to 30 inch size scales. Among these, chemical vapor deposition (CVD)[17] is regarded as one of the most promising techniques to produce relatively high quality large-area graphene sheets in a simple, easy and low cost manner, which is compatible for TCE for flexible optoelectronics.[10] For graphene to be useful in optoelectronic devices as a TCE it needs low sheet resistance and large light transmission. Most work to date has been optimizing graphene synthesis and devices on the 1cm scale, with only a few reports of growing graphene in sizes above 10cm and its detailed characterization. Upscaling growth from the 1-2inch tube furnace systems routinely used in most CVD experiments for graphene growth to larger 4inch and above is not trivial and more work is needed in exploring the factors that influence this upscaling process.

Recent results demonstrated a 100-meter-long graphene film by low pressure CVD using selective Joule heating.[20] The sheet resistance was reported to be comparable to that of the conventional CVD-grown graphene. A large scale low-pressure CVD process was

reported to produce monolayer graphene films with a diagonal size of up to 30 inches, along with a roll-to-roll transfer process to flexible plastics.[21] Vlassiouk *et al.* also reported a similar large scale (40 inches diagonal) graphene synthesis and studied the influence of copper foil morphology and its pretreatment.[22] However, a detailed analysis of the spatial uniformity of the samples were not thoroughly undertaken, which is important to see how the quality of the film varies on different size scales across the sample.

One approach for lowing the sheet resistance of graphene is to stack multiple layers one-by-one on top of each other to create a multi-layered film.[8,23–27] This can be time-consuming method to obtain bilayer graphene, whereas directly growing bilayer graphene by CVD on Cu could lead to reduced number of transfers and minimized cracks, residues and contamination during the layer by layer transfer, allowing for a more uniform graphene surface and better performance in TCE applications. In addition, bilayer graphene with Bernal (AB) stacking order has advantage over monolayer graphene in its tunable band structure, which allows the development of semiconducting graphene for device applications based on electronic bands.[28,29] Recent work on the CVD synthesis of bilayer graphene film has been reported by studying the catalyst substrate, concentration of carbon source, growth temperature and total pressure.[30–35] In particular, Lee et al.[33] reported a bilayer graphene film across 2inch by 2inch area grown on a copper sheet by CVD. A method of producing Bernal stacked bilayer graphene (3inch by 3inch) was introduced by Liu et al.[31] using CVD on engineered alloy catalyst films. The homogeneity of their films was evaluated by Raman mapping[31–35] and further supported by electrical transport measurements.[33,35]

In this work, we examine the upscale growth of large area (14cm x 6cm) graphene films on copper sheets by ambient pressure CVD within a 4 inch tube furnace system. The

quality of the graphene is measured by transferring onto Si substrates with 300nm oxide and also polyethylene terephthalate (PET) flexible films that are compatible with flexible TCE applications. The effect of different local gas flow conditions on film uniformity is investigated by altering the ceramic support used to hold the Cu catalyst. Bilayer graphene films with high coverage were successfully grown and characterized using Raman spectroscopy, scanning electron microscopy, van der Pauw measurements of sheet resistance and optical transmittance spectroscopy.

Results and discussion

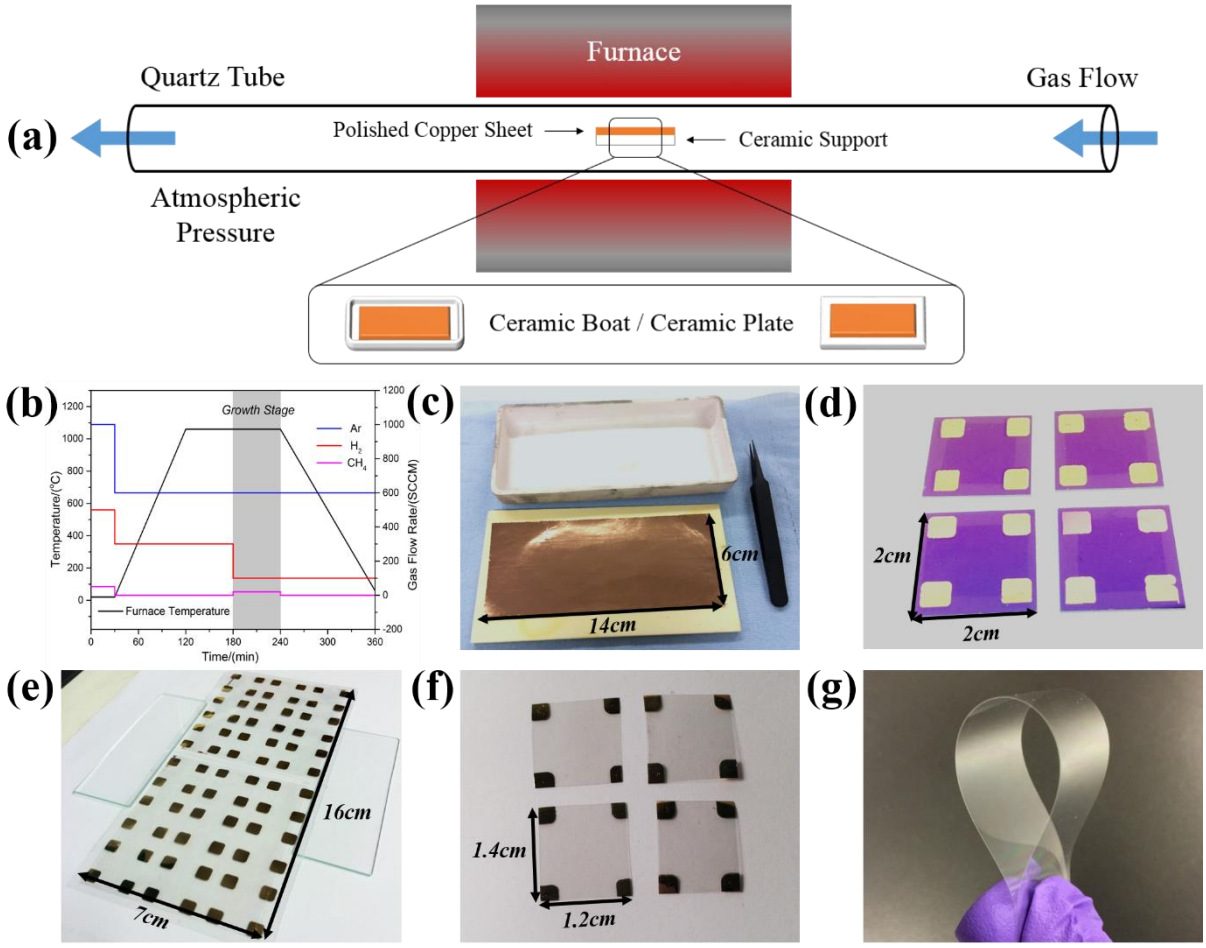

Figure 1. Atmospheric pressure CVD synthesis of large-area (14cm x 6cm) bilayer graphene on copper. (a) Schematic illustration of the CVD experimental set-up with polished copper sheet in a ceramic boat or a flat ceramic plate. (b) Temperature profiles of the furnace as a function of time and the gas flow rate of argon, hydrogen and methane during the growth, respectively. Black line: furnace temperature. Blue line: argon. Red line: hydrogen. Magenta line: methane. (c) Photo of large-area graphene sheet on copper. The photo also displays the ceramic boat and the ceramic plate used during the graphene synthesis. (d) Photo of four transferred graphene samples on SiO_2/Si with pre-patterned metal contacts. The SiO_2/Si we used here is 2cm by 2cm. (e) Photo of two large pieces of graphene sheet on pre-patterned PET substrates before PMMA removal. The area for each PET substrate is about 8cm by 7cm. (f) Photo of four transferred graphene samples on PET substrates with pre-patterned electrodes. The area of the PET varies from $1cm^2$ to $2cm^2$. (g) Photo of the flexible PET substrate used for transfer. The thickness is 5μm.

The synthesis of large area graphene was carried out using a custom built 4-inch CVD system with quartz tube and gas flow rates controlled by digital mass flow controllers. This builds on our prior experience of graphene growth on copper by CVD at the 1 inch scale.[36] Methane was introduced here as the gaseous carbon source and copper foil as the catalyst metal substrate. Figure 1(a) shows the schematic diagram of the 4-inch quartz tube atmospheric pressure CVD system with copper sitting on a ceramic support. The whole system was first flushed with argon, hydrogen and methane and then ramped up to a high temperature. The copper was annealed for at least one hour after the furnace reached the desired temperature. Graphene was then grown on copper by introducing the carbon source. In order to get a uniform bilayer graphene film with less grain boundaries and defects, the growth recipe in terms of argon/hydrogen/methane gas flow rate, growth temperature and growth time was evaluated and optimized. Figure 1(b) presents a temperature curve for the

furnace as a function of time and the gas flow rate used for growing bilayer graphene during each timeline. This allowed us to produce a large bilayer graphene sheet with size up to 14cm by 6cm, as shown in Figure 1(c). Before the samples were transferred onto SiO_2/Si or PET substrates using a standard wet transfer method, a layer of metal (10nm Chromium and 90nm Gold) was thermally evaporated onto all the substrates as electrodes. The samples transferred onto SiO_2/Si were cut into 40 pieces before wet etching. Figure 1(d) shows four of the graphene samples on SiO_2/Si. For the samples transferred onto PET, we first transferred one whole piece of graphene onto two big PET substrates, as shown in Figure 1(e). After removing the PMMA using acetone, the samples were then cut into 50 pieces for further characterization. Figure 1(f) shows four of the graphene samples that were transferred on PET. Figure 1(g) demonstrates the flexible nature of the thin PET film used for flexible TCE of graphene.

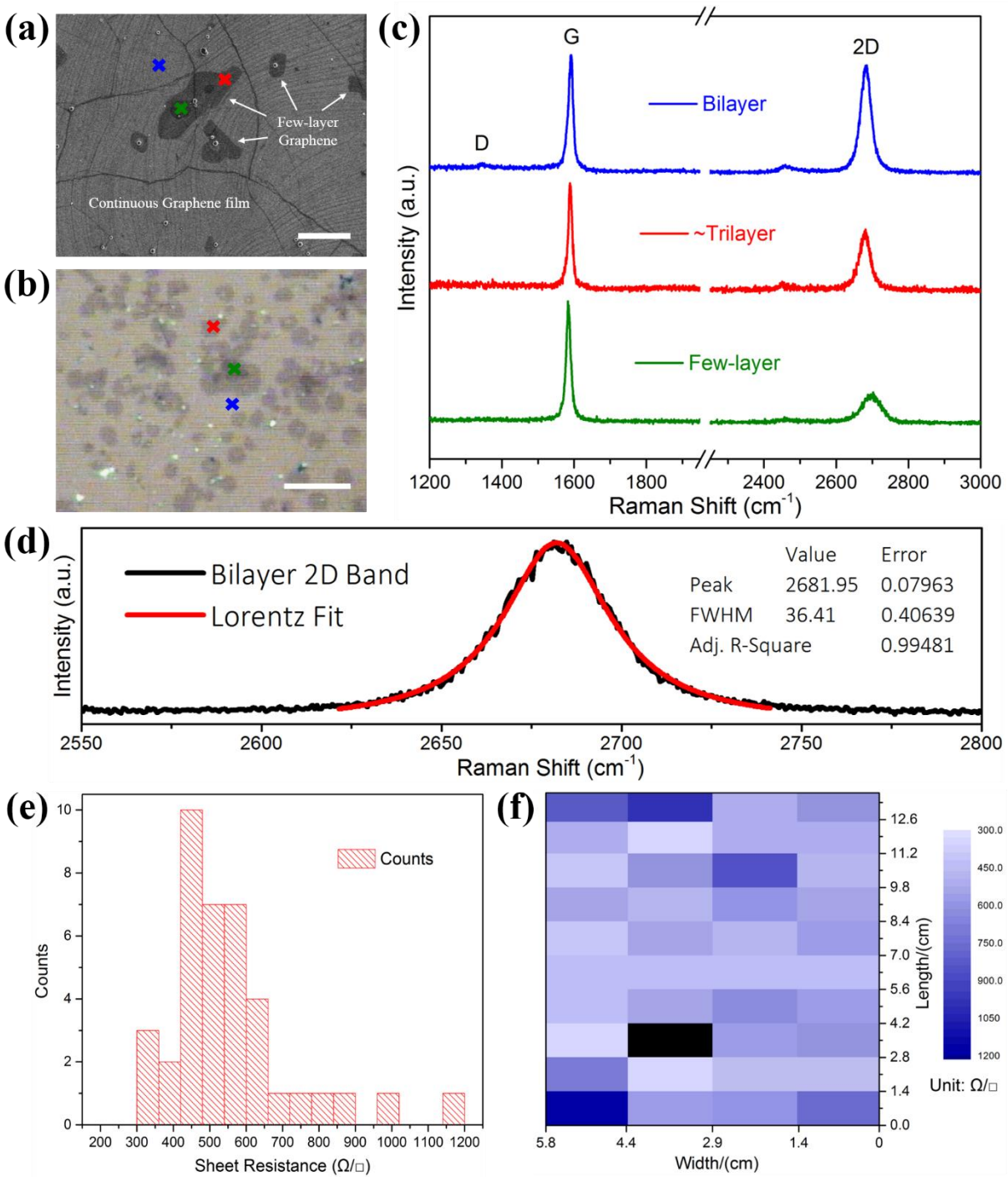

Figure 2. Characterization of graphene grown on Cu situated in a ceramic boat and then transferred to Si substrate with 300nm oxide layer. (a) SEM image of the continuous graphene film transferred from copper foil onto Si substrate with a 300nm-thick layer of SiO_2 showing grain boundaries, wrinkles as well as few layers of graphene areas. Scale bar: 5μm. (b) Optical image of the

graphene samples on SiO_2/Si. Scale bar: 20μm. (c) Raman spectra of the marked spots with corresponding colored crosses showing the existence of bi-, tri- and few-layer graphene. Blue line: bilayer graphene. Red line: ~trilayer graphene. Green line: few-layer graphene. (d) Lorentzian fitting of the 2D band in the Raman spectrum of bilayer graphene. Histogram (e) and spatial distribution (f) of sheet resistance of the graphene samples transferred onto SiO_2/Si. The black box indicates that the graphene sample there was broken after transfer.

Figure 2(a) and Figure 2(b) present some typical area of the transferred graphene on SiO_2/Si examined by SEM and optical microscopy, respectively. The non-uniform contrast indicates the variation of the film thickness. The graphene film is continuous with about 30% of the area containing smaller thicker graphene islands. Raman spectroscopy was used to evaluate the quality and interpret the thickness of the graphene film. Figure 2(c) shows the Raman spectra of three marked spots with different color in the panels (blue cross, red cross, green cross in Figure 2(a) and Figure 2(b)). All three spectra present the two important features related to graphene: a G peak at ~1590 cm^{-1} and a 2D peak at ~2690 cm^{-1}.[16,17,37] The 2D/G intensity ratio of the spectra in blue is ~1, which indicates bilayer graphene.[16,17,32,35] The red one with a ratio of ~0.7 indicates that the graphene is about 2-4 layers thick,[37] and the green one showing 2D/G ratio less than 0.3 represents few-layer (>4) graphene.[16] The D peak (~1350 cm^{-1}) used to identify the level of defects[38] in graphene was found to be negligible for all three spectra, implying the high quality of the transferred CVD graphene. As can be seen from Figure 2(d), the 2D band for our CVD-grown bilayer graphene is almost symmetrical and can be fitted as one Lorentzian peak, which is consistent with other reported results.[16,17] It indicates that most of the areas in our synthesized bilayer graphene film exhibit weak interlayer coupling[32] likely due to turbostratic stacking, which is different from AB Bernal stacking nearly always obtained from mechanically exfoliated bilayer graphene.[39]

Figure 2(e) shows the histogram of graphene sheet resistance, the mean and the standard deviation of which is 559.7Ω/□ and 171.9Ω/□, respectively, similar to other reported values.[20,40] Figure 2(f) shows a more straight-forward way to understand the distribution of the quality of transferred graphene on SiO_2/Si in terms of sheet resistance. From the sheet resistance results, we found that the thickness of the graphene grown at the corners of the ceramic boat is thinner and more likely to be broken than that of the others during the transfer process. This was reflected by the relatively higher sheet resistance values at corners and was thought to be caused by the comparatively lower methane concentration. The black box highlighted indicates an area damaged during the transfer process.

The turbostratic stacking revealed by Raman spectroscopy in figure 2(d), was further explored using aberration-corrected transmission electron microscopy to directly image the atomic structure of the bilayer graphene films. Rotational stacking faults manifest themselves as Moire patterns in the lattice images of few layer graphene films.[46] Most of the transferred films showed bilayer regions with turbostratic ordering. However, during the transfer of the bilayer graphene film, some areas were degraded and we found these regions to contain a boundary of monolayer-bilayer interface. This allows us to study the bilayer in more detail and also show that it is only 2 layers thick. Figure 3(a) shows an area of the sample containing a monolayer-bilayer interface. The yellow box in figure 3(a) contains the interface region and is show in higher magnification in figure 3(b). The fast Fourier transforms (FFTs) from the red and yellow boxes in figure 3(b) are from the monolayer and bilayer regions respectively and show the misorientation angle of 13^o between the two layers. An atomic model of a turbostratic bilayer with ~13^o angle is presented in figure 3(e) to show how the Moire pattern forms from the overlapping positions of the carbon atoms in each layer, where

each layer is given a different colour. We know that the region indicated by the red box in figure 3(b) is monolayer and not AB Bernal stacked multilayers because we followed this structure across to a region next to a hole in the film, indicated by the red box in figure 3(a). This area shows a single monolayer reaching the vacuum at the hole, figure 3(f), confirming monolayer thickness and subsequently confirming the turbostratic region as being bilayer. Figure 3(g) shows a large area region of the turbostratic bilayer graphene with a higher magnification image in figure 3(h) revealing the details of the Moire pattern. These results confirm the findings of the Raman spectroscopy that the bilayer graphene is predominantly turbostratic and not AB Bernal stacked.

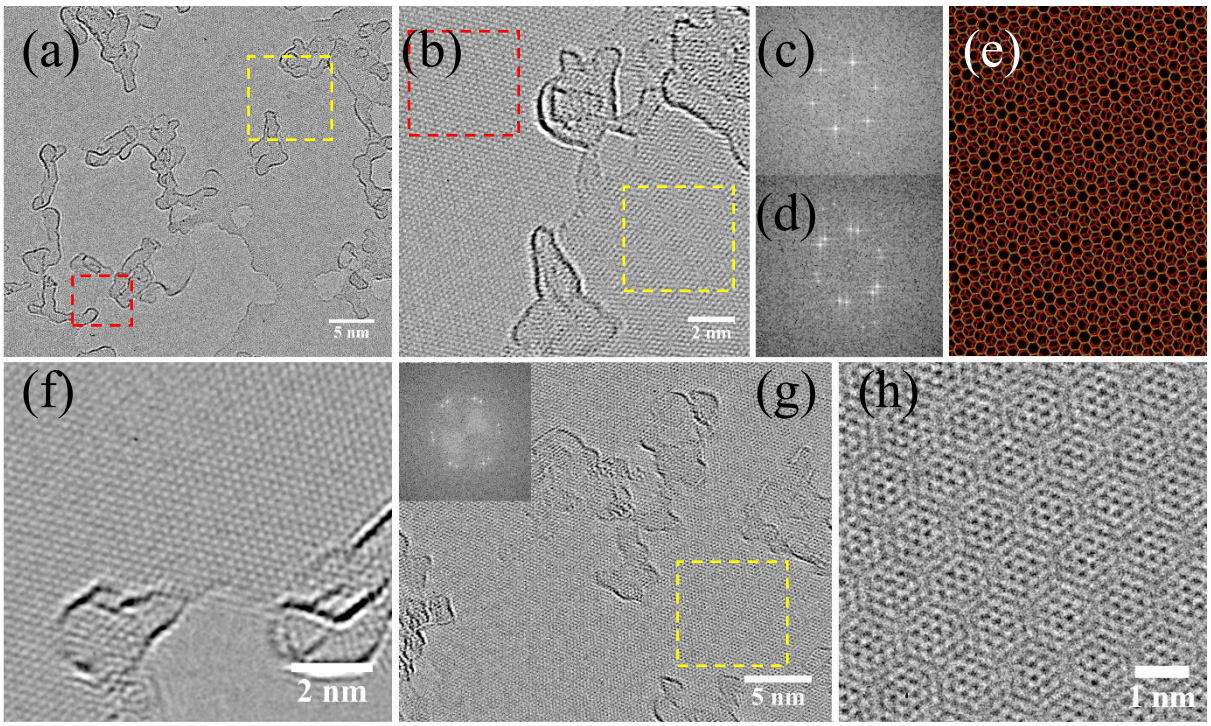

Figure 3. Atomic resolution imaging of bilayer graphene by aberration-corrected transmission electron microscopy. (a) AC-TEM image of a region where a monolayer-bilayer interface is found. (b) AC-TEM image from the region indicated with the yellow dashed box in (a) showing the monolayer-bilayer interface. (c) Fast Fourier transform (FFT) from the region indicated with the red

box in (b) corresponding to the single monolayer region. (d) FFT from the region indicated with the yellow box in (b) corresponding to the turbostratic bilayer region. Angle between spots is ~13^{o} (e) Atomic model of two graphene sheets with rotational angle of ~13^{o} to create a Moire pattern similar to those directly imaged in (b). (f) AC-TEM image of the region indicated by the red box in (a), corresponding to the edge of the monolayer graphene sheet near a hole. (g) AC-TEM image of the large area of turbostratic bilayer graphene showing Moire pattern. Inset shows the FFT from the entire image. (h) AC-TEM image of the area indicated by the yellow box in (g).

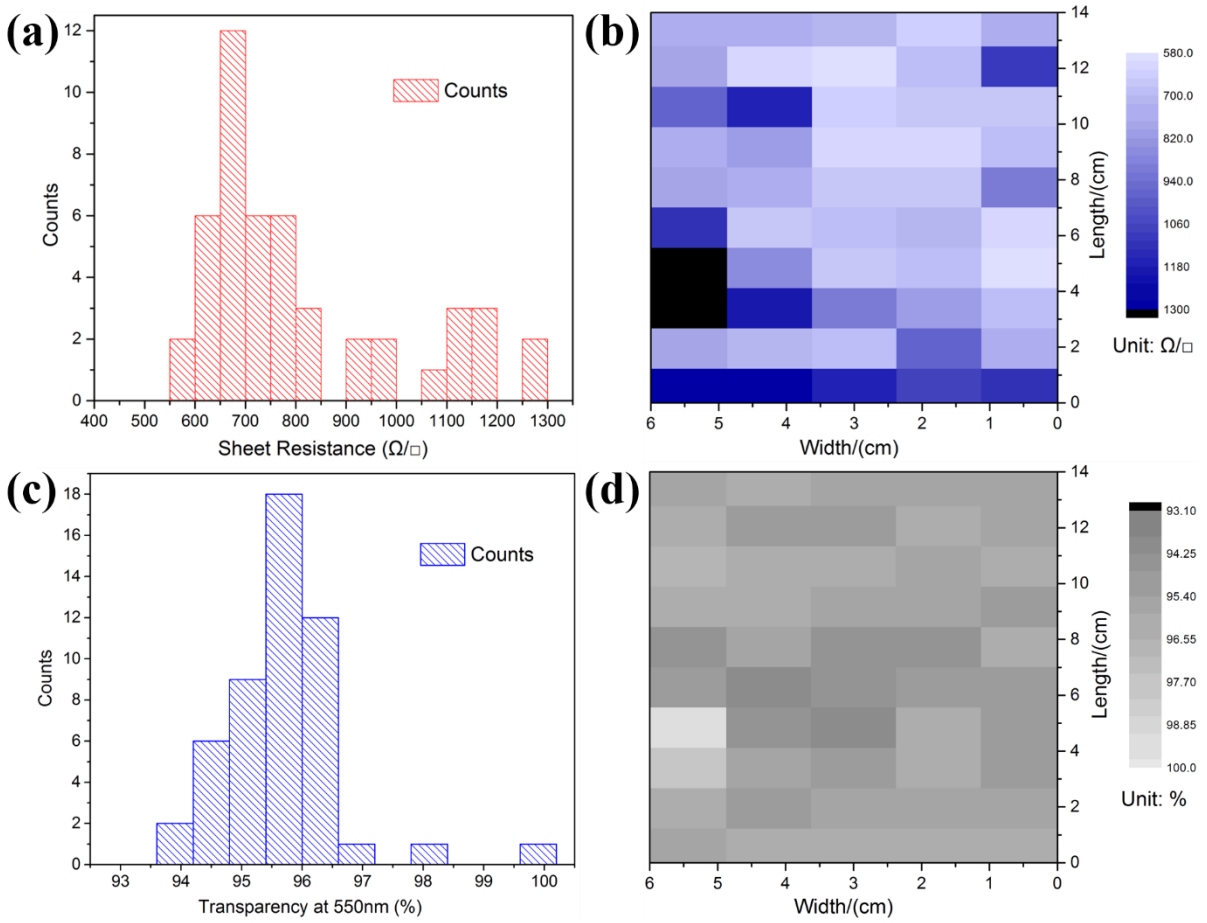

Figure 4. Characterization of graphene grown on Cu situated in a ceramic boat and then transferred to PET substrate. Histograms (a) and spatial distribution (b) of sheet resistance of the whole graphene sheet on PET. The two black boxes indicate that the graphene samples there were broken after transfer. Histogram (c) and spatial distribution (d) of optical transmittance of the large-area graphene at 550nm.

To further characterize the graphene fabricated when the copper was supported within a ceramic boat, we transferred another graphene sheet onto PET substrates and measured its combined sheet resistance and optical transmittance properties. It was reported that the theoretical value of optical transmittance of the single-layer graphene is about 97.7% and will

be decreased by ~2.3% when adding another layer.[5,41,42] For bilayer graphene, the optical transparency should be around 95.4%. Figure 4(c) and Figure 4(d) shows the histogram and spatial distribution of optical transmittance of the large-area graphene at 550nm, respectively. It shows a mean value of 95.7% with a standard deviation of 0.9%, which implies the graphene film is mostly bilayer. We also measured the sheet resistance of each graphene samples. Figure 4(a) shows the histogram of sheet resistance of all the graphene samples transferred onto PET, the average value of which is 808.2Ω/□ with a standard deviation 197.5Ω/□. Figure 4(b) presents the sheet resistance mapping of the graphene, from which we can find that the quality of the samples in first row is not as homogeneous as the others, indicating the possibility for producing more uniform graphene if we can improve the quality of graphene in the first row.

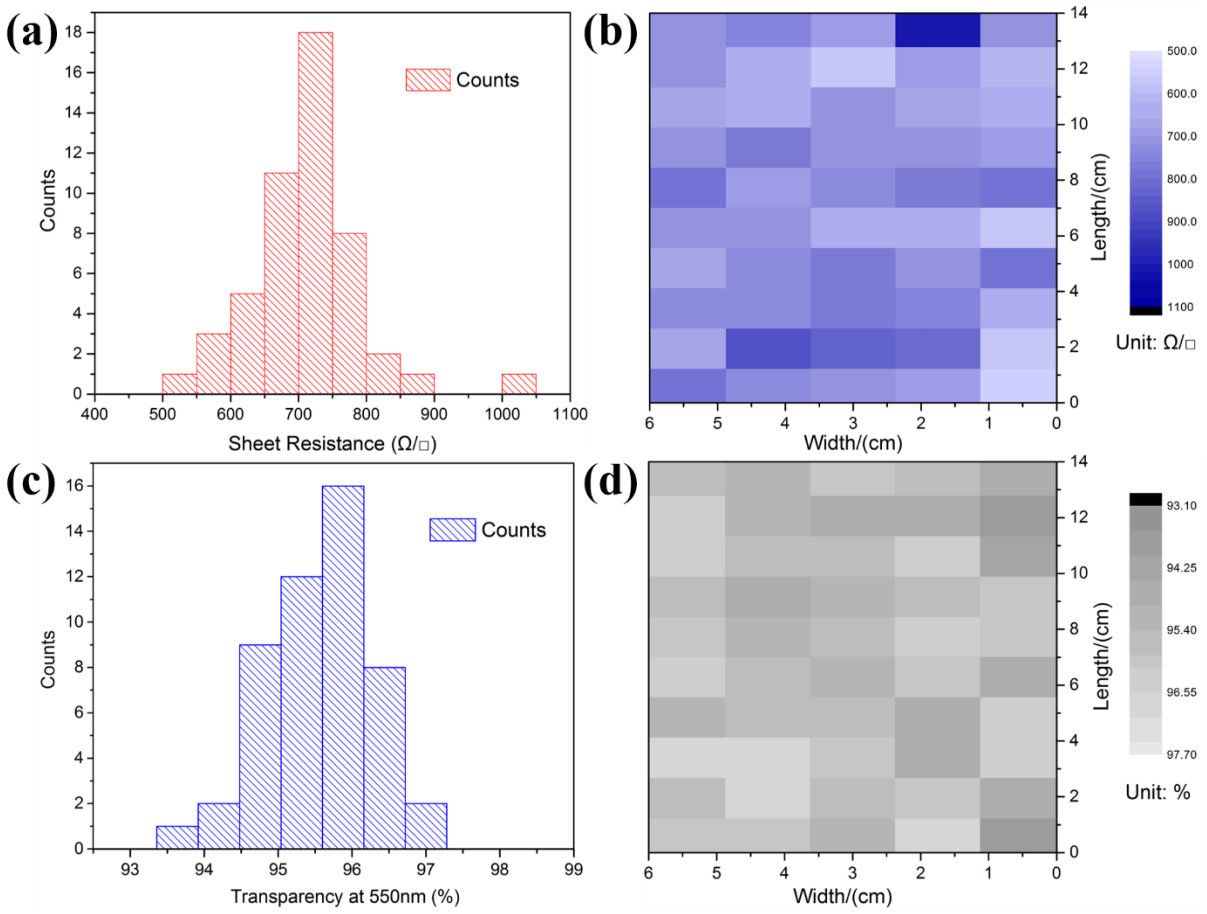

Figure 5. Characterization of graphene grown on Cu situated in a flat ceramic plate and then transferred to PET. Histogram (a) and spatial distribution (b) of the sheet resistance of the graphene on PET. Histogram (c) and mapping (d) of optical transmittance of the graphene samples on PET at 550nm.

The ceramic boat used to support the copper during CVD growth of graphene is likely to introduce some form of non-uniformity in the gas flow around its edges which will affect the quality of the graphene in terms of thickness and uniformity at the edges of the copper. To contrast this we replaced the ceramic boat with a flat ceramic plate and kept all other conditions the same during CVD growth of graphene. The flat ceramic plate should provide

more uniform gas flow conditions and deliver constant precursor to the entire copper sheet. Again, we prepared a piece of graphene film using the CVD system shown in Figure 1(a) with the same growth parameters and transferred the graphene onto PET substrates and measured its optical and electronic properties. Figure 5(c) and Figure 5(d) present the histogram and optical transmittance mapping of the transferred graphene film on PET, respectively. The transparency rate at 550nm mostly ranges from 94.9% to 96.3%. The average value is about 95.6%, which is closer to the theoretical value of bilayer graphene, with standard deviation is 0.7%, indicating a more uniform film. Figure 5(a) and Figure 5(b) show the histogram and spatial distribution of sheet resistance of the graphene samples transferred, respectively. The sheet resistance is mostly between 634.1 to 792.7Ω/□ with an average value of 713.4Ω/□. The standard deviation is ~79.3Ω/□, which is half of the one grown with a ceramic boat, indicating higher uniformity for the graphene film.

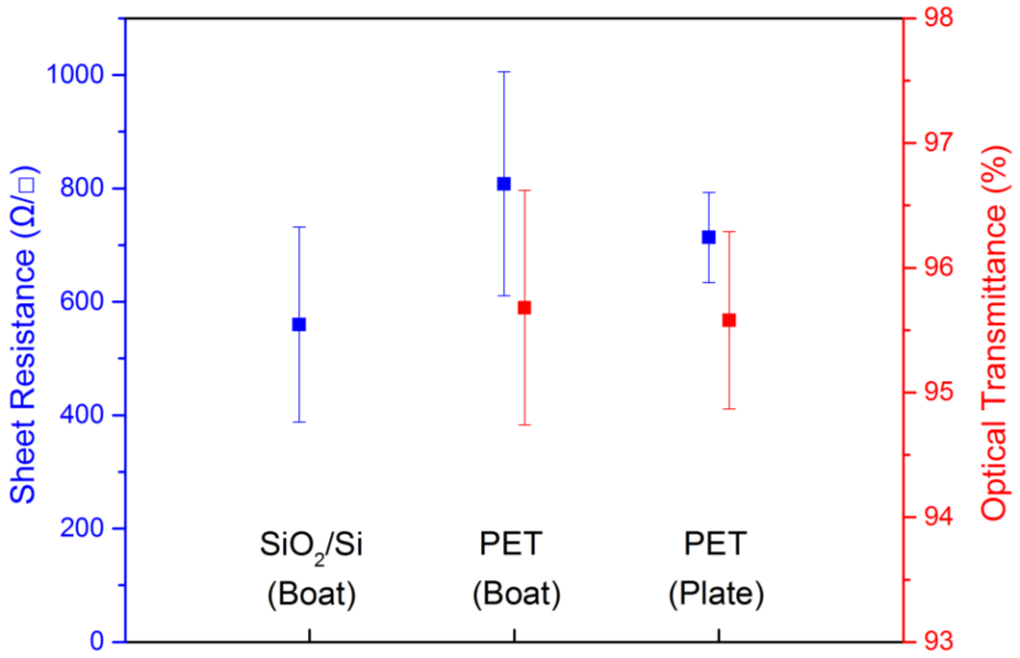

Figure 6. Correlated optical transmission at 550nm and sheet resistance values of graphene films on different substrates and grown with either the ceramic boat or flat plate. Blue dots: the average sheet resistance of graphene films on SiO_2/Si and PET. Red dots: the average optical transmittance values at 550nm of graphene samples on PET. Two of the graphene films were prepared in a ceramic boat and the other one was grown on a plate.

Figure 6 presents the comparison of graphene films on different substrates in terms of sheet resistance and optical transparency at 550nm. The average sheet resistance of graphene films transferred on SiO_2/Si is lower than the ones transferred on PET. This is likely due to the higher level of doping from the SiO_2/Si substrates compared to the PET.[43] The standard deviation of the sheet resistance for the two graphene films grown in the boat is similar, but much larger than the one grown on the plate, indicating the more uniform graphene film when using the plate during growth. The average transparency value at 550nm for the graphene film grown on the plate is slightly closer to the theoretical value of bilayer

graphene, compared with the one prepared in the boat. Similar to the sheet resistance case, the standard deviation of the transparency values for the samples grown on the plate is smaller than those fabricated in the boat, further confirming the conclusion that the uniformity of the graphene grown on the flat plate is better. The local gas flow dynamics above the sample during growth is thought to be the main factor that affects the uniformity of the large-area graphene films fabricated here. Laminar flow with lower Reynolds numbers is more preferred during the conventional CVD growth in a quartz tube.[44] For the growth with a flat plate, a smoother streamline is likely to form above the copper sheet. However, for the growth with a boat, the flow is disrupted by the irregular shape of the boat, which is more likely to result in turbulent flow above the sample. The introduced turbulent flow can cause pressure fluctuations over short areas and vortices can form at edges and corners, which may seriously influence the local growth environment for graphene synthesis. This leads to the growth of non-uniform graphene films with poorer electrical properties. In addition, the more even surface of the ceramic plate leads to a copper sheet with a flatter surface after annealing, resulting in a more homogeneous film.[45]

Conclusion

In summary, we prepared bilayer graphene sheets with areas up to 14cm by 6cm and studied the uniformity across the sample. The morphology and optoelectronic properties of the graphene films were characterized by SEM, TEM Raman spectroscopy, and sheet resistance and optical transmittance measurements, confirming that the graphene film is mostly bilayer with turbostratic stacking configurations. In particular we examined how different supporting substrates for the Cu catalyst impacted the final graphene films. Since both supports (boat and flat plate) have the same length, there is no difference in the

temperature variation between them inside the CVD system. Both the flat support and the boat shaped support will have the same temperature profiles. The only difference between the two supports is their shape, which will influence the gas flow dynamics. Therefore the poor growth of graphene at the edge of the films when using the boat is purely due to the turbulence of the gas flow, which is not present for the nice flat support. For the graphene films grown under turbulent local gas conditions (ceramic boat), we found that the quality in the center is better than edges and corners in terms of uniformity and continuity. The graphene film grown under more uniform local gas flow (ceramic plate) and was found to be much more homogeneous according to the sheet resistance and transparency measurements. It is anticipated that this study will facilitate the development of preparing large-area uniform bilayer graphene films and allow the mass-production of TCE for commercial applications in flexible and wearable electronics.

Methods

Synthesis of CVD graphene

A piece of 25μm thick 14cm by 6cm 99.8% copper (Goodfellow) was first polished by Brasso for at least 15 minutes. After that, oxides residues on the copper surface were removed through sonication in diluted hydrochloric acid (HCl) solution (1M) for two minutes, and then sonicated in acetone and isopropanol (IPA) for 5 minutes each. Finally, the whole piece of copper was put into a ceramic boat or a ceramic plate, and was then placed into an air tight 4-inch quartz tube. A horizontal tube furnace with accompanying control unit (Carbolite model HST 12/400) was moved to the sample's position by sliding it across mounted runners. In order to ensure a uniform temperature during growth, the copper sheet was positioned in the center of the furnace. Three gases (BOC) were used within the system:

1% methane in argon, 25% hydrogen in argon and 100% argon (hereinafter referred to as CH_4, H_2 and Ar). The flow rate of these gases could be individually controlled using Alicat mass flow controllers in conjunction with Flowvision computer software, and was measured in standard cubic centimeters per minute (sccm). The CVD growth was performed at atmospheric pressure and was first purged with 1000 sccm Ar, 500 sccm H_2 and 50 sccm CH_4 for 30 minutes. The temperature of the furnace was then set to 1060^{o}C at a ramping rate of 50^{o}C/min under a flow of 600 sccm of Ar and 300 sccm of H_2. The copper was annealed at 1060^{o}C with the same flow rate for 1 hour. Graphene growth was carried out at 1060 ^{o}C under a flow of 600 sccm of Ar, 100 sccm of H_2 and 20 sccm of CH_4 for 1 hour. After growth, the furnace was slide away from the sample to the other end of the runners, which allow the sample to be fast cooled to room temperature.

Transfer of graphene

After cooling process, the as-prepared graphene sample was first spin coated with a layer of 495K A8 Poly(methyl methacrylate) PMMA at 4500 rpm for 60 seconds using a spin coater (Laurell-WS-650MZ-23NPP), and then cured on a hot plate (Stuart-SD160) at 180^{o}C for 90 seconds to remove any anisole from the PMMA. The copper was etched away by floating the sample on an aqueous solution of $FeCl_3$ (1M). For the graphene samples transferred onto SiO_2/Si, the whole copper sheet was cut into 40 pieces before copper etching, while it was cut into two big pieces for the ones transferred onto PET. The PMMA/graphene stack was then washed in DI water for 30 minutes. This was followed with a 15 minutes floating atop a 1M HCl solution in order to remove any residual iron. The film was rinsed in DI water for three further times to wash away any remaining acid. After all the cleaning process, the sample was transferred onto a cleaned substrate, either SiO_2/Si or PET, with pre-patterned metal contact

and left in the fume hood overnight to slowly evaporate the water trapped between the film and the substrate. The sample was then baked on the hot plate at 150 ^{o}C for 15 minutes and placed in acetone for 2-3 hours to remove PMMA.

Characterization of graphene

The structural characteristics of the transferred graphene samples on SiO_2/Si were observed using a scanning electron microscope (Hitachi-4300) under an accelerating voltage of 3.0 kV. Raman spectroscopy was carried out using a JY Horiba LabRAM Aramis imaging confocal Raman microscope under an excitation wavelength of 532 nm. The sheet resistance was measured at least ten times per sample by van der Pauw technique, which was conducted by a home-made four-point probe equipment connected to a source meter (Keithley 2400V) under ambient conditions. An Ultraviolet-Visible-Near Infrared spectrometer (Jasco V-570) was used to determine the optical transparency of graphene samples on PET substrates in the wavelength range 400-700nm. Aberration-corrected transmission electron microscope (AC-TEM) was performed using the Oxford-JEOL JEM-2200MCO field-emission gun TEM with a CEOS imaging aberration corrector, operating at an accelerating voltage of 80 kV. Graphene was transferred onto a SiN TEM grid containing 2μm holes.

Reference

(1) Novoselov, K. S.; Geim, a K.; Morozov, S. V; Jiang, D.; Zhang, Y.; Dubonos, S. V; Grigorieva, I. V; Firsov, a a. Electric Field Effect in Atomically Thin Carbon Films. *Science* **2004**, *306*, 666–669.

(2) Geim, a K.; Novoselov, K. S. The Rise of Graphene. *Nat. Mater.* **2007**, *6*, 183–191.

(3) Allen, M. J.; Tung, V. C.; Kaner, R. B. Honeycomb Carbon: A Review of Graphene. *Chem. Rev.* **2010**, *110*, 132–145.

(4) Bolotin, K. I.; Sikes, K. J.; Jiang, Z.; Klima, M.; Fudenberg, G.; Hone, J.; Kim, P.; Stormer, H. L. Ultrahigh Electron Mobility in Suspended Graphene. *Solid State Commun.* **2008**, *146*, 351–355.

(5) Wu, W.; Yu, Q.; Peng, P.; Liu, Z.; Bao, J.; Pei, S.-S. Control of Thickness Uniformity and Grain Size in Graphene Films for Transparent Conductive Electrodes. *Nanotechnology* **2012**, *23*, 035603.

(6) Balandin, A. a; Ghosh, S.; Bao, W.; Calizo, I.; Teweldebrhan, D.; Miao, F.; Lau, C. N. Superior Thermal Conductivity of Single-Layer Graphene. *Nano Lett.* **2008**, *8*, 902–907.

(7) Lin, Y.-M.; Dimitrakopoulos, C.; Jenkins, K. A.; Farmer, D. B.; Chiu, H.-Y.; Grill, A.; Avouris, P. 100-GHz Transistors from Wafer-Scale Epitaxial Graphene. *Sci.* **2010**, *327* , 662.

(8) Bae, S.; Kim, H.; Lee, Y.; Xu, X.; Park, J.-S.; Zheng, Y.; Balakrishnan, J.; Lei, T.; Ri Kim, H.; Song, Y. Il; *et al.* Roll-to-Roll Production of 30-Inch Graphene Films for Transparent Electrodes. *Nat Nano* **2010**, *5*, 574–578.

(9) Schwierz, F. Graphene Transistors. *Nat Nano* **2010**, *5*, 487–496.

(10) Bonaccorso, F.; Sun, Z.; Hasan, T.; Ferrari, A. C. Graphene Photonics and Optoelectronics. *Nat Phot.* **2010**, *4*, 611–622.

(11) Han, T.-H.; Lee, Y.; Choi, M.-R.; Woo, S.-H.; Bae, S.-H.; Hong, B. H.; Ahn, J.-H.; Lee, T.-W. Extremely Efficient Flexible Organic Light-Emitting Diodes with Modified Graphene Anode. *Nat Phot.* **2012**, *6*, 105–110.

(12) Wu, J.; Agrawal, M.; Becerril, H. A.; Bao, Z.; Liu, Z.; Chen, Y.; Peumans, P. Organic Light-Emitting Diodes on Solution-Processed Graphene Transparent Electrodes. *ACS Nano* **2009**, *4*, 43–48.

(13) Kim, K. S.; Zhao, Y.; Jang, H.; Lee, S. Y.; Kim, J. M.; Kim, K. S.; Ahn, J.; Kim, P.; Choi, J.; Hong, B. H. Large-Scale Pattern Growth of Graphene Films for Stretchable Transparent Electrodes. *Nature* **2009**, *457*, 706–710.

(14) Sutter, P. W.; Flege, J.-I.; Sutter, E. a. Epitaxial Graphene on Ruthenium. *Nat. Mater.* **2008**, *7*, 406–411.

(15) Stankovich, S.; Dikin, D. a.; Piner, R. D.; Kohlhaas, K. a.; Kleinhammes, A.; Jia, Y.; Wu, Y.; Nguyen, S. T.; Ruoff, R. S. Synthesis of Graphene-Based Nanosheets via Chemical Reduction of Exfoliated Graphite Oxide. *Carbon N. Y.* **2007**, *45*, 1558–1565.

(16) Reina, A.; Jia, X.; Ho, J.; Nezich, D.; Son, H.; Bulovic, V.; Dresselhaus, M. S.; Kong, J. Large Area, Few-Layer Graphene Films on Arbitrary Substrates by Chemical Vapor Deposition. *Nano Lett.* **2009**, *9*, 30–35.

(17) Li, X.; Cai, W.; An, J.; Kim, S.; Nah, J.; Yang, D.; Piner, R.; Velamakanni, A.; Jung, I.; Tutuc, E.; *et al.* Large-Area Synthesis of High-Quality and Uniform Graphene Films on Copper Foils. *Science* **2009**, *324*, 1312–1314.

(18) Berger, C.; Song, Z.; Li, X.; Wu, X.; Brown, N.; Naud, C.; Mayou, D.; Li, T.; Hass, J.; Marchenkov, A. N.; *et al.* Electronic Confinement and Coherence in Patterned Epitaxial Graphene. *Science* **2006**, *312*, 1191–1196.

(19) Eda, G.; Fanchini, G.; Chhowalla, M. Large-Area Ultrathin Films of Reduced Graphene Oxide as a Transparent and Flexible Electronic Material. *Nat. Nanotechnol.* **2008**, *3*, 270–274.

(20) Kobayashi, T.; Bando, M.; Kimura, N.; Shimizu, K.; Kadono, K.; Umezu, N.; Miyahara, K.; Hayazaki, S.; Nagai, S.; Mizuguchi, Y.; *et al.* Production of a 100-M-Long High-Quality Graphene Transparent Conductive Film by Roll-to-Roll Chemical Vapor Deposition and Transfer Process. *Appl. Phys. Lett.* **2013**, *102*, 023112.

(21) Bae, S.; Kim, H.; Lee, Y.; Xu, X.; Park, J.-S.; Zheng, Y.; Balakrishnan, J.; Lei, T.; Kim, H. R.; Song, Y. Il; *et al.* Roll-to-Roll Production of 30-Inch Graphene Films for Transparent Electrodes. *Nat. Nanotechnol.* **2010**, *5*, 574–578.

(22) Vlassiouk, I.; Fulvio, P.; Meyer, H.; Lavrik, N.; Dai, S.; Datskos, P.; Smirnov, S. Large Scale Atmospheric Pressure Chemical Vapor Deposition of Graphene. *Carbon N. Y.* **2013**, *54*, 58–67.

(23) Li, X.; Zhu, Y.; Cai, W.; Borysiak, M.; Han, B.; Chen, D.; Piner, R. D.; Colombo, L.; Ruoff, R. S. Transfer of Large-Area Graphene Films for High-Performance Transparent Conductive Electrodes. *Nano Lett.* **2009**, *9*, 4359–4363.

(24) Kim, K. K.; Reina, A.; Shi, Y.; Park, H.; Li, L.-J.; Lee, Y. H.; Kong, J. Enhancing the Conductivity of Transparent Graphene Films via Doping. *Nanotechnology* **2010**, *21*, 285205.

(25) Wang, H.; Maiyalagan, T.; Wang, X. Review on Recent Progress in Nitrogen-Doped Graphene: Synthesis, Characterization, and Its Potential Applications. *ACS Catal.* **2012**, *2*, 781–794.

(26) Gunes, F.; Shin, H.; Biswas, C.; Han, G. H.; Kim, E. S.; Chae, S. J. Layer-by-Layer Doping of Few-Layer Graphene Film. **2010**, *4*, 4595–4600.

(27) Kasry, A.; Kuroda, M. a; Martyna, G. J.; Tulevski, G. S.; Bol, A. a. Chemical Doping of Large-Area Stacked Graphene Films for Use as Transparent, Conducting Electrodes. *ACS Nano* **2010**, *4*, 3839–3844.

(28) Oostinga, J. B.; Heersche, H. B.; Liu, X.; Morpurgo, A. F.; Vandersypen, L. M. K. Gate-Induced Insulating State in Bilayer Graphene Devices. *Nat. Mater.* **2008**, *7*, 151–157.

(29) Ohta, T.; Bostwick, A.; Seyller, T.; Horn, K.; Rotenberg, E. Controlling the Electronic Structure of Bilayer Graphene. *Science* **2006**, *313*, 951–954.

(30) Liu, W.; Li, H.; Xu, C.; Khatami, Y.; Banerjee, K. Synthesis of High-Quality Monolayer and Bilayer Graphene on Copper Using Chemical Vapor Deposition. *Carbon N. Y.* **2011**, *49*, 4122–4130.

(31) Liu, W.; Kraemer, S.; Sarkar, D.; Li, H.; Ajayan, P. M.; Banerjee, K. Controllable and Rapid Synthesis of High-Quality and Large-Area Bernal Stacked Bilayer Graphene Using Chemical Vapor Deposition. *Chem. Mater.* **2014**, *26*, 907–915.

(32) Luo, Z.; Yu, T.; Shang, J.; Wang, Y.; Lim, S.; Liu, L.; Gurzadyan, G. G.; Shen, Z.; Lin, J. Large-Scale Synthesis of Bi-Layer Graphene in Strongly Coupled Stacking Order. *Adv. Funct. Mater.* **2011**, *21*, 911–917.

(33) Lee, S.; Lee, K.; Zhong, Z. Wafer Scale Homogeneous Bilayer Graphene Films by Chemical Vapor Deposition. *Nano Lett.* **2010**, *10*, 4702–4707.

(34) Sun, H. Bin; Wu, J.; Han, Y.; Wang, J. Y.; Song, F. Q.; Wan, J. G. Nonisothermal Synthesis of AB-Stacked Bilayer Graphene on Cu Foils by Atmospheric Pressure Chemical Vapor Deposition. *J. Phys. Chem. C* **2014**, *118*, 14655–14661.

(35) Liu, L.; Zhou, H.; Cheng, R.; Yu, W. J.; Liu, Y.; Chen, Y.; Shaw, J.; Zhong, X.; Huang, Y.; Duan, X. High-Yield Chemical Vapor Deposition Growth of High-Quality Large-Area AB-Stacked Bilayer Graphene. *ACS Nano* **2012**, *6*, 8241–8249.

(36) Wu, Y. A.; Fan, Y.; Speller, S.; Creeth, G. L.; Sadowski, J. T.; He, K.; Robertson, A. W.; Allen, C. S.; Warner, J. H. Large Single Crystals of Graphene on Melted Copper Using Chemical Vapor Deposition. *ACS Nano* **2012**, *6*, 5010–5017.

(37) Lui, C. H.; Li, Z.; Chen, Z.; Klimov, P. V; Brus, L. E.; Heinz, T. F. Imaging Stacking Order in Few-Layer Graphene. *Nano Lett.* **2010**, *11*, 164–169.

(38) Ferrari, A. C.; Meyer, J. C.; Scardaci, V.; Casiraghi, C.; Lazzeri, M.; Mauri, F.; Piscanec, S.; Jiang, D.; Novoselov, K. S.; Roth, S.; *et al.* Raman Spectrum of Graphene and Graphene Layers. *Phys. Rev. Lett.* **2006**, *97*, 187401.

(39) Ferrari, A. C. Raman Spectroscopy of Graphene and Graphite: Disorder, Electron–phonon Coupling, Doping and Nonadiabatic Effects. *Solid State Commun.* **2007**, *143*, 47–57.

(40) Suk, J. W.; Kitt, A.; Magnuson, C. W.; Hao, Y.; Ahmed, S.; An, J.; Swan, A. K.; Goldberg, B. B.; Ruoff, R. S. Transfer of CVD-Grown Monolayer Graphene onto Arbitrary Substrates. *ACS Nano* **2011**, *5*, 6916–6924.

(41) Nair, R. R.; Blake, P.; Grigorenko, a N.; Novoselov, K. S.; Booth, T. J.; Stauber, T.; Peres, N. M. R.; Geim, a K. Fine Structure Constant Defines Visual Transparency of Graphene. *Science* **2008**, *320*, 1308.

(42) Kuzmenko, A.; van Heumen, E.; Carbone, F.; van der Marel, D. Universal Optical Conductance of Graphite. *Phys. Rev. Lett.* **2008**, *100*, 117401.

(43) Lafkioti, M.; Krauss, B.; Lohmann, T.; Zschieschang, U.; Klauk, H.; Klitzing, K. V.; Smet, J. H. Graphene on a Hydrophobic Substrate: Doping Reduction and Hysteresis Suppression under Ambient Conditions. *Nano Lett.* **2010**, *10*, 1149–1153.

(44) Hong, B. H.; Lee, J. Y.; Beetz, T.; Zhu, Y.; Kim, P.; Kim, K. S. Quasi-Continuous Growth of Ultralong Carbon Nanotube Arrays. *J. Am. Chem. Soc.* **2005**, *127*, 15336–15337.

(45) Han, G. H.; Güneş, F.; Bae, J. J.; Kim, E. S.; Chae, S. J.; Shin, H. J.; Choi, J. Y.; Pribat, D.; Lee, Y. H. Influence of Copper Morphology in Forming Nucleation Seeds for Graphene Growth. *Nano Lett.* **2011**, *11*, 4144–4148.

(46) Warner, J. H.; Ruemmeli, M. H.; Gemming, T.; Beuchner, B.; Briggs, G. A. D.; Direct Imaging of Rotational Stacking Faults in Few Layer Graphene, *Nano Lett*, **2009**, 9, 102-106